Physics of Plasmas

Are we ready to transfer optical light to gamma-rays?

Cite as: Phys. Plasmas **26**, 053103 (2019); https://doi.org/10.1063/1.5090992
Submitted: 31 January 2019 . Accepted: 20 April 2019 . Published Online: 13 May 2019

M. Vranic, T. Grismayer, S. Meuren, R. A. Fonseca, and L. O. Silva

Physics of Plasmas ARTICLE scitation.org/journal/php

Are we ready to transfer optical light to gamma-rays?

Cite as: Phys. Plasmas **26**, 053103 (2019); doi: 10.1063/1.5090992
Submitted: 31 January 2019 · Accepted: 20 April 2019 ·
Published Online: 13 May 2019

M. Vranic,[1,a),b)] T. Grismayer,[1] S. Meuren,[2] R. A. Fonseca,[1,3] and L. O. Silva[1,c)]

AFFILIATIONS

[1]GoLP/Instituto de Plasmas e Fusão Nuclear, Instituto Superior Técnico-Universidade de Lisboa, 1049-001 Lisbon, Portugal
[2]Department of Astrophysical Sciences, Princeton University, Princeton, New Jersey 08544, USA
[3]DCTI/ISCTE Instituto Universitário de Lisboa, 1649-026 Lisbon, Portugal

Note: This paper is part of the Special Collection: Papers from the 60th Annual Meeting of the APS Division of Plasma Physics.
Note: Paper BI3 5, Bull. Am. Phys. Soc. **63** (2018).
[a)]Invited speaker.
[b)]**Electronic mail:** marija.vranic@ist.utl.pt
[c)]**Electronic mail:** luis.silva@ist.utl.pt

ABSTRACT

Scattering relativistic electrons with optical lasers can result in a significant frequency upshift of photons, potentially producing γ-rays. This is what linear Compton scattering taught us. Ultra-intense lasers offer nowadays a new paradigm where multiphoton absorption effects come into play. These effects can result in higher harmonics, higher yields, and also electron-positron pairs. This article intends to discriminate the different laser scenarios that have been proposed over the past few years as well as to give scaling laws for future experiments. The energy conversion from lasers or particles to high-frequency photons is addressed for both the well-known counter propagating electron beam-laser interaction and quantum-electrodynamics cascades triggered by various lasers. Constructing bright and energetic gamma-ray sources in controlled conditions is within an ace of seeing the light of day.

I. INTRODUCTION

Ultra-intense laser-matter interactions can generate γ-rays. Several recent experiments have obtained hard X-rays in the laboratory using counter-propagating electron beams and laser pulses.[1–5] A review on laser-wakefield acceleration (LWFA)-based light sources summarizes other viable configurations for generating energetic photons and the properties of radiation that could be obtained with a reflection to prospective applications.[6]

Multiphoton Thompson scattering was observed in a recent experiment by Yan *et al.*[7] The next goal is to obtain a high conversion efficiency of the electron energy into high-frequency radiation. This requires operating the source in a regime of significant radiation recoil, in the classical or quantum regime of interaction. First evidence of electron slowdown in a laser field[8,9] is consistent with the classical radiation reaction predictions for scattering a LWFA electron bunch and a laser pulse.[10] However, there are still many open questions regarding the transition from the classical to the quantum radiation reaction dominated regime, which has generated keen interest in the last few years.[11–18]

The radiation reaction dominated regime (i.e., the regime where particles lose a substantial amount of energy through radiation emission) can be reached either by using higher laser intensities or more energetic electrons. The particles in this regime emit either a few very energetic photons (quantum radiation reaction) or a large number of low-energy photons successively (classical radiation reaction).[19] The currently published energy record for LWFA electrons is 4 GeV, and those electrons are obtained using a 16 J laser.[20] In the next generation laser facilities, electron energies on the order of 10 GeV are expected. Pairing such electron beams with intense lasers can provide access to more extreme regimes of interaction. It may even be possible to obtain multiple electron-positron pairs from electron beam-laser collision. In the two-step approximation, a particle first emits a high-energy photon, which then decays into an electron-positron pair via the Breit-Wheeler (BW) process in an intense electromagnetic background. A milestone experiment was performed at SLAC,[21] where BW pairs were produced in a collision of a 46.6 GeV electron beam from a linear accelerator with a green laser at the intensity of $\sim 10^{18}$ W/cm^2. The next generation of laser facilities is expected to deliver a much higher

pair yield[22,23] even using electrons with lower energies (on the order of a few giga-electronvolts). Further laser-electron scattering experiments are planned, relying on both LWFA and conventional accelerators to provide the electrons.

Another way to generate γ-rays and pairs with intense lasers is QED cascades.[19,24] One of the most popular configurations is to use two colliding lasers to create an intense standing wave[25–30] whose nonlinear evolution in the presence of self-generated plasma can be studied theoretically resorting to QED-PIC simulations (particle-in-cell simulations incorporating a Monte Carlo algorithm for quantum processes).[28,31–38] New laser facilities will access extreme regimes of interaction[39–42] where we can expect an abundance of electron-positron pairs. This motivated much theoretical effort to improve our understanding of QED cascades, considering configurations using multiple lasers,[43–45] as well as the challenges concerning the cascade seeding.[46,47] Among the proposed solutions for the seeding problem, it was proposed to use solid targets.[48,49] Configurations with nanowires were also proposed to enhance the laser heating of the target electrons.[50]

In this manuscript, we focus on the gamma-ray emission. We revisit the two main configurations: laser-electron beam scattering and the two-laser QED cascade. The first aim is to connect the hard photon emission in both these scenarios and bring an intuitive understanding of why even in a QED cascade, the classical absorption is more important than the instantaneous quantum absorption. The ratio of the classical and quantum absorption has been found previously using QED calculations[51] to be proportional to the square of the local normalized vector potential a_0, where $a_0 = 0.86\sqrt{I[10^{18}\,\mathrm{W/cm^2}]}\,\lambda\,[\mu\mathrm{m}]$ for linearly polarized lasers and $a_0 = 0.61\sqrt{I[10^{18}\,\mathrm{W/cm^2}]}\lambda\,[\mu\mathrm{m}]$ for circular polarization. In other words, this ratio is proportional to the laser intensity, and for high laser intensities, the classical absorption dominates. Here, we show how the electron-photon scattering in a QED cascade can be mapped to a simple laser-electron scattering scenario for which the quantum vs classical absorption ratio has already been calculated. The second aim is to estimate how much energy is converted to hard photons in both configurations and identify the relevant regimes of interaction. We also give a brief summary of the scaling laws for evolution of the electron energy distribution function in the laser-electron beam scattering. This is of importance for planning of experiments because the electron beam properties imprint on the emitted radiation. The ideas and scalings presented in this manuscript are relevant for the multipetawatt laser projects such as ELI,[39] Apollon,[52] and CoReLS[53] that aim to reach unprecedented laser intensities, as well as FACET-II[54] and LUXE[55,56] that plan to perform laser scattering experiments using 10 GeV-class high-quality electron beams.

This manuscript is organized as follows. In Sec. II, we discuss the ratio of classical vs quantum absorption in a scattering of a single electron with one wave. We mostly discuss the counter-propagating geometry because it provides the highest energy photons. We then extend the ideas presented for a single wave-electron interaction to a lepton interacting with a standing wave formed by two colliding lasers. Later we review the scaling laws and the energy conversion expected for the electron-laser scattering configuration. We finally discuss the radiative absorption in a two-laser cascade. We distinguish two regimes: a regime of controlled radiation emission, when the wave is not severely affected by the presence of the plasma, and a regime where the plasma density is high enough to disrupt the wave (this can occur because the target is dense in the beginning or due to the considerable production of electron-positron pairs). We identify the parameters where the pair production is low enough to operate a controlled γ-ray source in a low-absorption regime with solid hydrogen targets already available in the laboratory. The results are supported with QED-PIC simulations for a range of parameters, in both 2D and 3D geometries.

II. QUANTUM LASER ABSORPTION VS CLASSICAL LASER ABSORPTION

Quantum vs classical laser absorption by a single electron was first considered by Meuren *et al.*[51,57] using the QED formalism. Here, we provide an intuitive picture for the corresponding scaling laws.

A. Laser-electron scattering

The first studies dealing with interaction of electrons with intense laser beams date back to a few years after the invention of the laser.[58,59] It was found that a mass change induced in the electron (considered initially at rest) by the external field of the laser shifts the wavelength of the scattered photons by an amount depending on the intensity of the incident beam. Furthermore, the absorption of multiple laser photons becomes possible, which facilitates the emission of harmonics. If the electron is initially relativistic, the scattering with the laser photons can result in the emission of γ-rays.

Effectively, only a finite space-time region is relevant for the photon emission process. It is characterized by the so-called formation length l_f that depends on the wave intensity[60]

$$\frac{l_f}{\lambda} \sim \frac{1}{a_0}, \tag{1}$$

where λ is the wavelength of the wave. Equation (1) is valid for $\chi_e \lesssim 1$, where the definition of the quantum parameter for electrons counter-propagating with an optical laser ($\lambda = 1\,\mu$m) can be approximated as $\chi_e \simeq 5\times10^{-6}\gamma_0 a_0$.

According to Eq. (1), the radiation is formed over multiple laser cycles if $a_0 \ll 1$. In this regime, it is useful to introduce the so-called "dressed momentum" for the emitting electron, which is obtained by averaging the classical canonical momentum over a laser period.[58,60,61] Correspondingly, the classical mass change mentioned above appears.

For $a_0 \gg 1$, we have $l_f \ll \lambda$ and the radiation process occurs almost instantaneously in an effectively constant background field. The concept of dressed momentum in this regime becomes meaningless.[51,57,62] Instead, a semiclassical approximation becomes possible, i.e., the radiating electron follows a classical trajectory between localized emission events.[63,64]

In this regime, we can distinguish two types of energy transfers: classical and quantum absorption.[51,57] The term quantum laser absorption ϵ_{LQ} is defined as the direct contribution of the laser photons that scatter with the electrons during the quasi-instantaneous emission process. Any laser absorption that occurs elsewhere (the laser energy invested in the electron acceleration) can be described classically and is incorporated into the instantaneous electron energy contribution ϵ_e. The analysis of the energy transfer from electrons to photons allows estimating the importance of quantum laser absorption during the electron interaction with an intense laser beam.

The scattering process is affected by the presence of the intense laser field in two ways. One aspect is that there is a temporary momentum transfer from the laser to the electrons: the laser induces electron oscillations. A relativistic electron counter-propagating toward an

intense laser with normalized vector potential a_0 acquires an additional transverse momentum on the order of $\sim a_0 mc$ during the interaction, while the effect on the longitudinal momentum is small if $a_0 \ll \gamma_0$. For circular polarization, the additional electron transverse momentum is constant in magnitude but periodically changes the direction revolving around the propagation axis, while for linear polarization, the direction is fixed, but the magnitude changes periodically. The second effect of the very intense field to the scattering process is that the local field energy density is high, which means that there can be many photons within the interaction volume. Such a photon density allows us to have frequent repeated scatterings as well as to absorb more than one photon at a time in a single scattering.

The following paragraph illustrates intuitively, by comparing the typical timescales of acceleration and emission, how the factor a_0^2 between the classical and quantum photon absorption might arise. Let us assume that $a_0 \gg 1$, and the particle emits a hard photon not more than once during one full laser cycle. The photon formation time is $\tau_f = l_f/c$, where c is the speed of light. The laser period is T_L. As $T_L/\tau_f \sim a_0$, the total work of the laser electric field during one period on one particle is a_0 times larger than that during one emission event. However, at relativistic intensities, an electron can take much more energy from the wave, on the order of $\xi \sim a_0^2 mc^2$ (assuming that the electron is initially at rest). This is because a relativistic electron can have a longer effective interaction time, and one oscillation can last longer than a simple laser period T_L (for example, if an electron copropagating with the wave). From there, we get that $T_{\text{eff}} \sim a_0 T_L$ and $T_{\text{eff}}/\tau_f \sim a_0^2$. One should note that the value of T_{eff} depends on the initial particle energy and the scattering angle, but it is never smaller than $T_L/2$. If we have n emissions during one laser cycle, then the average time between two emissions is T_{eff}/n. The relevant ratio then becomes $T_{\text{eff}}/(n\tau_f) \sim a_0^2/n$. If a particle is counter-propagating with a wave, then most of the energy of the emitted photons is invested by the electron. However, the laser has to invest a few photons (even if not many) into the electron acceleration (classically) and also during the actual emission event in order to facilitate it (quantum absorption). One can show that the classical vs quantum absorption of the laser photons scales as a_0^2. As the quantum absorption is negligible for $a_0 \gg 1$, it is not considered in the QED-PIC algorithms. However, the classical absorption that occurs due to the laser interaction with the plasma particles (i.e., particle acceleration) is intrinsically included in the PIC algorithm.

B. Mapping photon emission in a QED cascade produced by two colliding lasers with the photon emission in laser-electron scattering

The ideas presented for a laser-electron scattering do not trivially port to the standing wave configurations with multiple lasers. Particles can be initially at rest. The particles first get accelerated, then lose energy due to radiation emission, and then get re-accelerated[65] by the electric field in the standing wave. All the energy radiated to high-frequencies comes from the laser field: either through accelerating the electrons (classical absorption) or by providing photons for scattering to occur (quantum absorption). The question is: which channel is dominant?

We can make use of what we know about particle dynamics in a standing wave to establish a connection between this setup and the simple laser-electron scattering discussed in Sec. II A. Electrons (and positrons) gain momentum on the order of a_0, that is, perpendicular to the laser propagation axis.[34,47,65] In the case of circular polarization, leptons keep rotating, always remaining perpendicular to the laser propagation. This allows for a simplified consideration as the laser-photon scattering always occurs at the right angle.

If the particle scatters with photons from only one laser, the situation is exactly the same as a scattering with one laser at 90°. However, in principle, we could have a linear combination of m photons from one wave and n photons for the other participating in the scattering (not every combination is necessarily allowed, but here we assume a most general case). As the particle Lorentz factor is typically on the order of a_0, the energy of an individual photon in the particle rest frame is $\xi'_{ph} \sim a_0\, \xi_{ph}$, regardless of which laser the photon belongs to. Furthermore, the photons of both waves practically copropagate in the electron rest frame as the Lorentz boost gave them a momentum in the same direction. In other words, the electron sees them almost as one wave, apart from the tiny difference in the momentum ($\sim$1 eV for optical photons) perpendicular to the boost direction [see Fig. 1(d)].

Particle dynamics is slightly different when we have linearly polarized laser pulses forming the standing wave. The electric field is perpendicular to the laser propagation axis, but the magnetic field then rotates the momentum, and the particles can be found counter-propagating with one of the waves. In the electron rest frame, counter-propagating photons are upshifted, while the photons of the copropagating laser are downshifted. The most energetic photons in the electron rest frame are the counter-propagating ones. We can then see the analogy with the laser-electron scattering emerging naturally as one wave becomes more important than the other. We note here that the normalized vector potential a_0 is Lorentz-invariant, which means that the wave with higher energy individual photons in the electron instantaneous rest frame has a higher energy density. There is a range of possible angles of incidence, with two limiting cases: particles being perpendicular to the laser propagation axis or counter-propagating with one of the lasers [see Fig. 1(e)]. In general, any of these configurations can be mapped to an electron-laser scattering.

We have not discussed a decay of a hard photon into a pair here because the number of emission events in a QED cascade surpasses the number of pair production events by orders of magnitude. They contribute little to the overall energy balance. Nevertheless, it was shown in Ref. 51 that the ratio between the classical and quantum laser absorption for pair production is also $\epsilon_{CL}/\epsilon_{LQ} \sim a_0^2$.

III. SCALING LAWS FOR LASER-ELECTRON SCATTERING

In a collision between an intense laser and an electron beam, the final electron energy after the interaction can be estimated as[10]

$$\gamma_F \simeq \frac{\gamma_0}{1 + k\gamma_0} \tag{2}$$

for $k < 1$. The coefficient k depends on the laser duration τ_0 at FWHM and peak intensity I_0 in the following way:

$$k = 3.2 \times 10^{-5}\, I_{22}\, \tau_0[\text{fs}]\, (1 - \cos\theta)^2, \tag{3}$$

where $I_{22} = I_0[10^{22}\ \text{W/cm}^2]$ and θ represents the angle of interaction (for counter-propagation, $\cos\theta \simeq -1$). The counter-propagating

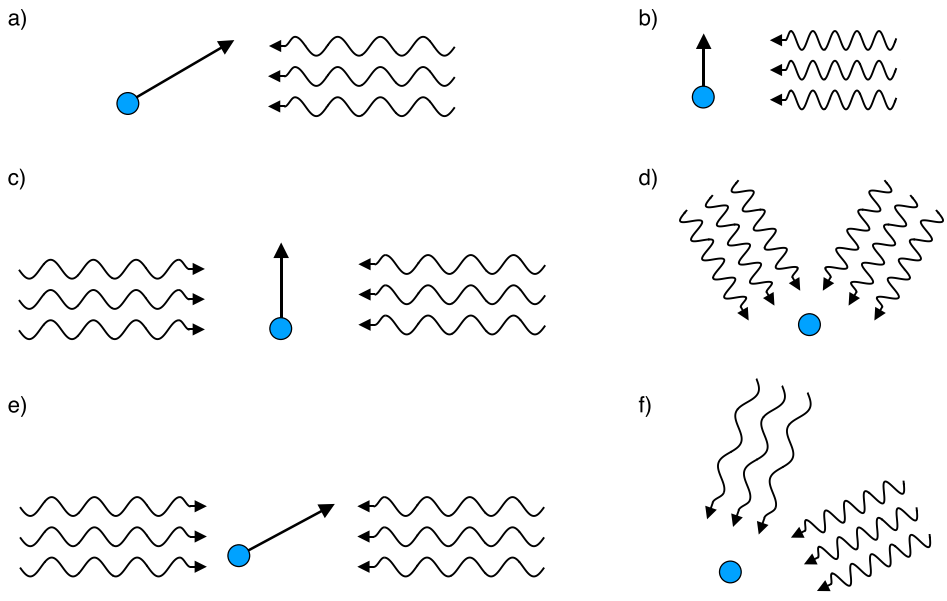

FIG. 1. Geometry of the interaction in laboratory (left-hand side) and boosted frames (right-hand side). (a) and (b) Laser-electron head-on configuration; (c) and (d) two laser standing wave, when interacting particle instantaneous momentum is perpendicular to the laser axis; (e) and (f) two laser standing wave interacting with a particle at an oblique angle.

configuration, therefore, corresponds to the strongest radiation reaction or losing a largest fraction of the electron energy. The energy converted to photons is then approximately

$$\xi_{rad}[mc^2] \simeq \frac{k\gamma_0^2}{1+k\gamma_0}. \tag{4}$$

Note that the electron beam energy bandwidth is bound to rise due to stochasticity in the quantum regime $\chi_e \gtrsim 1$.[11,12] But the high-energy electrons, on average, radiate more than low-energy electrons. This tends to reduce the energy bandwidth, even in the quantum regime of interaction. The electron distribution function either spreads or shrinks depending on the local conditions. In the limit where the scattering is still Thompson in the electron rest frame, one can derive an expression for an instantaneous "turning point."[16] If the standard deviation of the electron energy distribution function σ is larger than σ_T, then the electron distribution function shrinks. For $\sigma < \sigma_T$, stochasticity dominates and the bandwidth of the electron energy distribution rises. The value of σ_T is given by[16]

$$\sigma_T[mc^2] \simeq 1.4\times10^{-2}\,\gamma_T^{3/2}\,I_{22}^{1/4}, \tag{5}$$

where γ_T is the average value of the instantaneous electron Lorentz factor. The validity of Eqs. (2) and (5) can be extended to the regime where $\chi_e \approx 1$ by adding a correction for the electron Gaunt factor.[17,18] However, the final expression then becomes more complex, and our aim here is to keep the scaling laws as simple as possible. The simplicity allows us to estimate an asymptotic energy spread[16] as a function of the initial electron energy γ_0 and the laser intensity and duration

$$\sigma_F[mc^2] \lesssim \left(\frac{1.5\times10^{-4}I_{22}^{1/2}\,\gamma_0^3}{\left(1+6.1\times10^{-5}\gamma_0\,I_{22}\,\tau_0[\mathrm{fs}]\right)^3}\right)^{1/2}. \tag{6}$$

Equation (6) is useful for planning experiments because it allows for a quick estimate of the expected final width of the electron energy distribution function. One can also predict the final divergence of the beam. Let us define the divergence as the average deflection angle θ_F from the main axis of beam propagation. In this case, one can estimate this value as

$$\theta_F \simeq \sqrt{\frac{2}{\pi}}\,\frac{a_0}{\gamma_F^2}\,\sigma_F. \tag{7}$$

Comparisons of Eq. (7) with QED-PIC simulations are given in Fig. 2. The blue dashed line represents the θ_F obtained using values of γ_F and σ_F, Eqs. (2) and (6). The red line represents the values obtained with Eq. (7), but using σ_F and γ_F measured in the simulation. The electron beam initial energy was 0.85 GeV, and it interacted with a circularly polarized laser of $a_0 = 27$. All other simulation parameters are given in the Appendix.

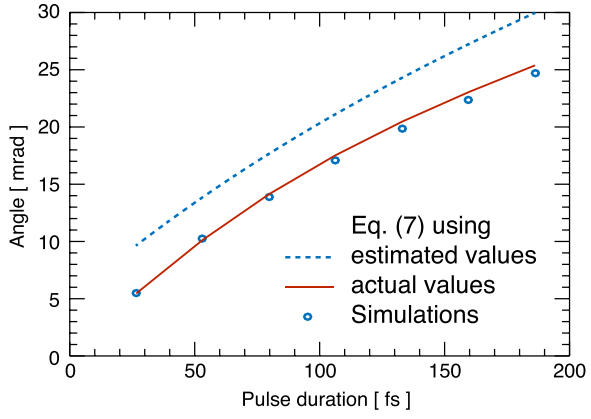

FIG. 2. Electron beam divergence after the shutdown of the interaction with the laser given in Eq. (7) and from simulations.

IV. ENERGY CONVERSION TO HIGH-FREQUENCY LIGHT IN A TWO-LASER STANDING WAVE (LINEAR POLARIZATION)

The number of photons of a plane wave with the normalized vector potential a_0 in a volume of λ_0^3 can be estimated as

$$N_{ph} = \frac{E^2}{4\pi}\lambda_0^3 \frac{1}{\hbar\omega_0} = \frac{a_0^2 a_S^2 2\pi^2}{\alpha} \simeq 3\times 10^{14} a_0^2. \quad (8)$$

Here, $a_S = mc^2/\hbar\omega_0 = 4.12\times 10^5\,\lambda_0\,[\mu\mathrm{m}]$ represents the Schwinger critical field in units normalized to the laser frequency. In other words, this defines the dimensionless normalized vector potential that corresponds to a Schwinger field at a given wave frequency. For our calculation, the total number of available photons in a volume of λ_0^3 given in Eq. (8) should be multiplied by a factor of 2 as the standing wave is formed by two counter-propagating traveling waves.

The temporal structure of the standing wave causes a periodic emission with a period of T_L. The constructive interference for the magnetic and electric field is temporally spaced at $T_L/4$. Periods of particle acceleration (when E is large) and rotation (when B dominates) therefore alternate every $T_L/4$. The characteristic cycle of emission is $T_L/2$ with the second half of the laser period repeating exactly the same particle dynamics in the opposite direction of motion.

Particle trajectories are chaotic,[66,67] and stochastic emission does not allow for a general analytical estimate of the radiated energy using the trajectories alone. However, average energy absorbed per particle during the half-period $T_L/2$ can be approximated using ideal simulations where pair production and current deposition are suppressed (see Figs. 3 and 4). In such simulations, the wave is not disturbed by the presence of the plasma. Photons do not decay into pairs, but the particles do experience quantum radiation reaction due to the hard photon emission.

The energy emitted by one particle during $T_L/2$ in an undisturbed linearly polarized standing wave with $\lambda_0 = 1\,\mu$m can be approximated as

$$\Delta\gamma \approx 9\times 10^{-4} a_0^2 + 0.2 a_0. \quad (9)$$

Equation (9), obtained as a best fit to the available data, can then be used to estimate the importance of radiative laser absorption for nonideal scenarios. What we mean by radiative absorption is the energy that was transferred from the laser to the particles through classical acceleration and then radiated to hard photons. When the standing wave interacts with a plasma target, this is one of the possible depletion channels.

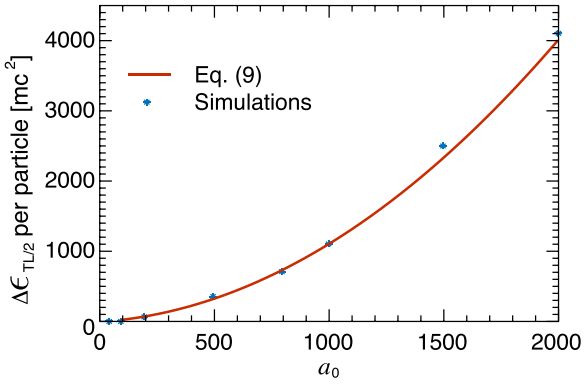

FIG. 3. Energy emitted per particle in an undisturbed standing wave during half of a laser period $T_L/2$. The line is given in Eq. (9), and points are obtained from simulations.

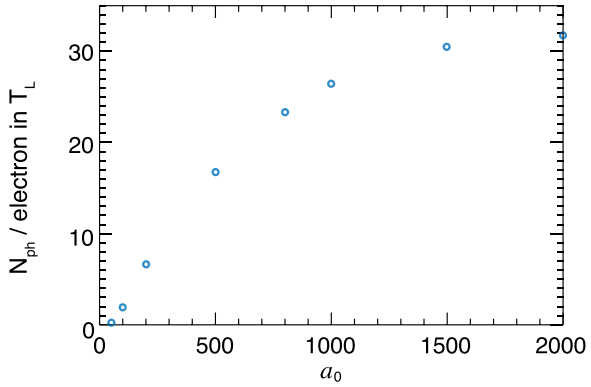

FIG. 4. Number of photons with energy above 1 MeV emitted during one laser period T_L per particle (electron or positron). The numbers are given for the undisturbed standing wave.

Let us assume that our target is 1 μm thick and the density n is much lower than the relativistic critical density $a_0 n_c$. In that case, we do not expect the standing wave to be disturbed. Also, by taking a narrow plasma slab, all plasma electrons (and eventually positrons) are located within one laser wavelength. This limits the interaction of each section of the traveling waves with the plasma to one full laser period. The radiative laser depletion can therefore be estimated locally in a λ_0^3 volume and during one full laser cycle. The percentage of the wave turned into high-frequency radiation depends on the local plasma density and the local laser intensity. The density gives an estimate of the total number of particles in the λ_0^3 volume, while the emitted energy per particle depends on the laser intensity and is given in Eq. (9).

If $n = n_c$ and we consider an electron-positron plasma, we have about 10^9 electrons and 10^9 positrons in the λ_0^3 volume. The fraction of the laser energy absorbed locally during one laser period is then given by

$$\left(\frac{\Delta\epsilon}{\epsilon}\right)_{T_L} \approx 3.3\, a_S \times 10^{-6}\left(\frac{n}{n_c}\right)\frac{(9\times 10^{-4} a_0 + 0.2)}{a_0}\times 4. \quad (10)$$

Here, multiplication factor 4 comes from moving from half of T_L to a full T_L and considering two species: electrons and positrons. If we now follow any point of the individual traveling waves at the speed of light as they pass the interaction region, we note that any absorption that occurs to that portion of the waves occurs within one T_L. The rest of the time, the wave propagates freely. Every T_L, there is a fresh portion of the wave interacting with the plasma, while the previous has escaped the interaction region. This means that the ratio given in Eq. (10) is approximately equal to the global absorption of the wave after the shutdown of the interaction.

For optical lasers with $\lambda_0 = 1\,\mu$m, interacting with a pair plasma, we observe that in an undisturbed standing wave, the energy converted to high-frequency radiation can be approximated as

$$\left(\frac{\Delta\epsilon}{\epsilon}\right) \approx \frac{3\times(9\times10^{-4}a_0+0.2)}{a_0}\left(\frac{n}{n_c}\right). \quad (11)$$

This estimate is not the whole picture because we neglect the self-consistent fields in the plasma and pair production. However, Eq. (11) allows us to estimate how strong is the high-frequency emission as a depletion channel when considering plasma densities much lower than the relativistic critical density $a_0 n_c$. Figure 5 illustrates the strong radiative absorption limit as a function of intensity as predicted by Eq. (11). The characteristic density is calculated for each laser intensity assuming 10% laser absorption and solving for n. If we would like to remain in the regime of low absorption (undisturbed wave), we have to use the density below this limit. It is interesting to note that one does not need to reach the relativistic critical density for extreme absorption according to this. For $a_0 = 1000$, even $n = 160 n_c$ is enough for strong absorption. Cryogenic targets available in experiments have a density on the order of 10 n_c, which means that it is possible to use them for controlled radiation sources, provided that the QED cascade does not increase the plasma density by an order of magnitude.

To evaluate a parameter range where this is the case, we should also analyze the pair production. Plasma density in a cascade increases exponentially: $n = n_0 \exp(\Gamma t)$, where Γ is a growth rate that depends on the laser intensity. For $a_0 < 500$, and circularly polarized lasers, the growth rate has an approximate expression given by[47]

$$\frac{\Gamma_{CP}}{\omega_0} = 2.6\times10^{-3} a_0 \exp\left(-\frac{2a_S}{3a_0^2}\right). \quad (12)$$

The growth rate predicted using Eq. (12) is in agreement with the recent calculations by Kostyukov *et al.*[68] for $a_0 \lesssim 400$. An upper estimate for linear polarization can be estimated by assuming that the same total energy yields the same growth rate. This is equivalent to using $a_0/\sqrt{2}$ instead of a_0 in Eq. (12)

$$\frac{\Gamma_{LP+}}{\omega_0} = 1.8\times10^{-3} a_0 \exp\left(-\frac{4a_S}{3a_0^2}\right). \quad (13)$$

Another option for Gaussian laser pulses is to insert $a_0/2$ instead of a_0 in Eq. (12) to account for the fact that not all particles experience the instantaneous maximum intensity

$$\frac{\Gamma_{LP-}}{\omega_0} = 1.3\times10^{-3} a_0 \exp\left(-\frac{8a_S}{3a_0^2}\right). \quad (14)$$

Using $a_0/2$ is also more consistent with the data obtained from cascade simulations at higher intensities[29,47] ($a_0 > 1000$). Equations (13) and (14) define a range of values for the expected growth rate at each a_0 for linear polarization. We should note here that near-threshold pair production is very sensitive to the seeding,[46,47,69] and so one may not be always able to reach the given growth rates. When using laser pulses, the actual growth rate is likely to be closer to Γ_{LP-} than to Γ_{LP+}. For example, the multiplicity we get for a 24.5 fs laser pulse with a peak intensity of $a_0 = 500$ using Eq. (14) is 1.44, while the simulation data give 1.69. For the same data, the upper bound Γ_{LP+} predicts a multiplicity of ~100, which is two orders of magnitude higher. Using an infinite plane wave, the multiplicity in the simulation increases, but it remains on the same order as predicted by Γ_{LP-} in Eq. (14). The growth rate estimates for $a_0 < 500$ given in Eqs. (12)–(14) are illustrated in Fig. 6.

As we mentioned before, for designing a radiation source, it may be favorable to keep the pair production rate low and operate in a more controlled emission regime. To avoid the uncertainty of seeding, it is also important to have a reliable estimate regarding how many particles are contained within the interaction volume. In this sense, using a gas jet would not be optimal even though it has an advantage of offering a possibility to start at a low density. A dense solid target can be manufactured to high precision, but then an undisturbed standing wave interaction is not possible. The best option available to date could be to use cryogenic targets, composed of hydrogen ice. They have recently been used in ion acceleration experiments, and a micrometer-level thickness was achieved[70,71] at a density of ~10 n_c.

In the following paragraphs, we consider the output radiation generated by interaction of two pulses with one such target, initially composed of electrons and protons. For completeness, we compare also the findings with the case when the target is initially composed of electrons and positrons, as well as the case when the standing wave is undisturbed. A range of intensities between $a_0 = 100$ and $a_0 = 1500$ was considered.

Figure 7 displays the angular distribution of radiation for all the cases, while Fig. 8 shows the conversion efficiency of optical light to

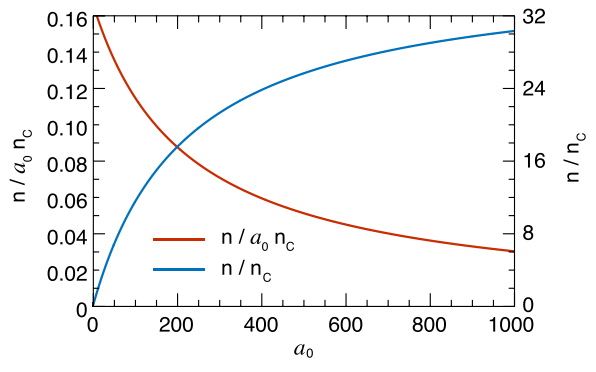

FIG. 5. Target density for strong absorption as a function of laser intensity. The target density is calculated when Eq. (11) predicts 10% absorption. For controlled conditions, one should aim at least one order of magnitude lower initial target density.

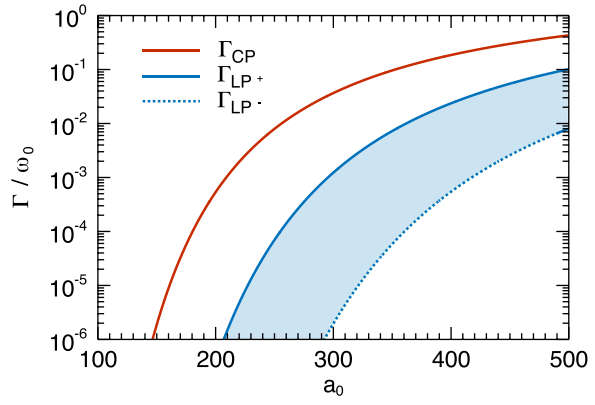

FIG. 6. Pair production growth rates for circular and linear polarization given in Eqs. (12)–(14).

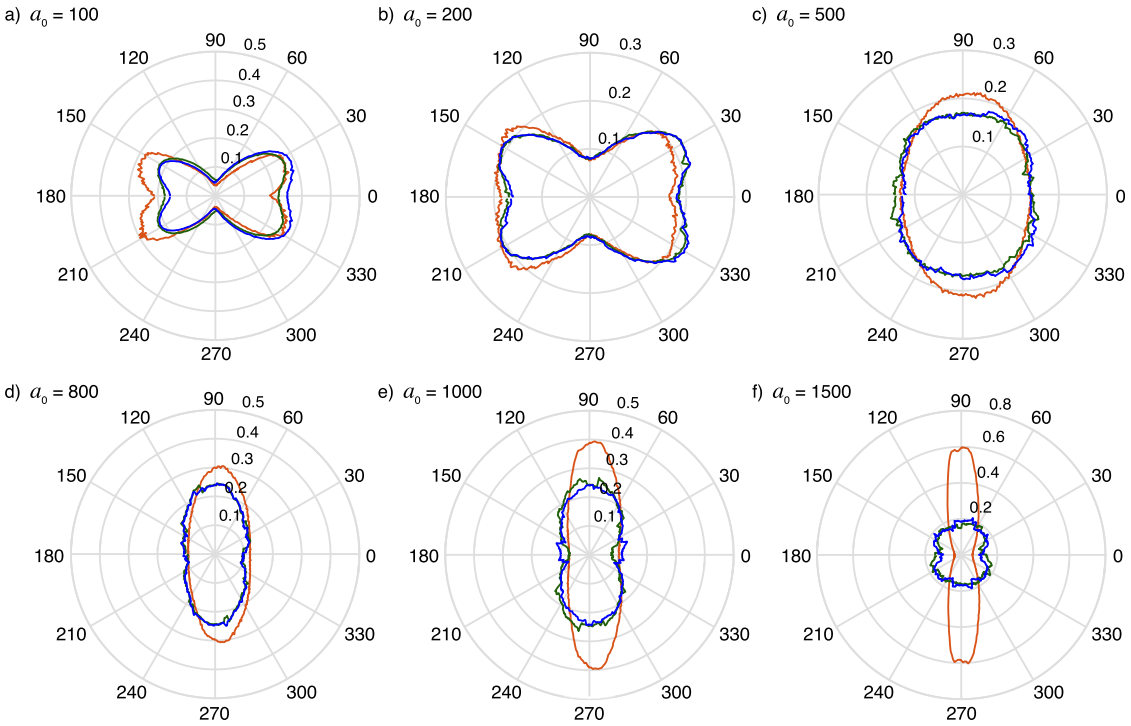

FIG. 7. Angular distribution of radiation as a function of intensity. The values of the radius represent a fraction of total energy radiated in a given direction per 1 rad (i.e., isotropic radiation would correspond to a circle with a radius of $1/2\pi$). The red curves correspond to the radiation in an undisturbed standing wave. The other two curves correspond to the radiation pattern obtained using a 10 n_c target composed of (green) electrons and positrons or (blue) electrons and protons.

high-frequency radiation. The differences between the electron-proton and electron-positron target in the typical radiation directions are almost negligible although there is a difference in the energy conversion efficiency. This is not surprising because in the electron-positron target, there are twice as many radiating leptons. The angular distribution in an undisturbed standing wave is quite different at some intensities compared to that of the 10 n_c target. For $a_0 = 100$, the 10 n_c target represents already 10% of the relativistic critical density for such a wave. Some level of discrepancy is therefore expected for the lower end of the explored intensities. At higher intensities, the discrepancies come from the pair production that increases the target density during the interaction until the density is high enough for wave disruption. The mid-range intensity of $a_0 \sim 500$ seems to be the best choice for controlled emission because the pair multiplicity is low, and at the same time, the intensity is high enough not to be too disturbed by the presence of the target.

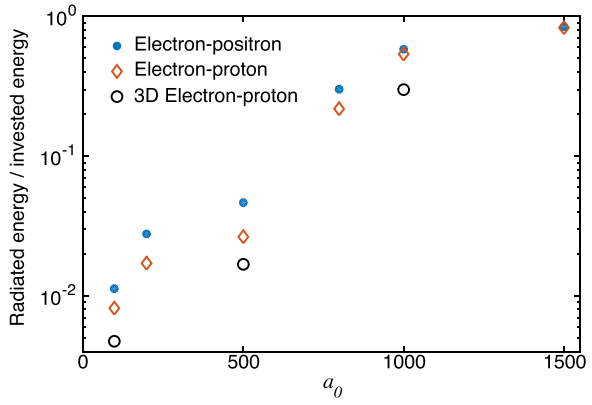

FIG. 8. Conversion efficiency of laser energy to emitted radiation using a 1 μm-thick target with an initial density of 10 n_c. The results shown are for a target composed of electrons and positrons (blue dots) or electrons and protons (red diamonds).

Figure 9 shows a 3D simulation using a cryogenic target for $a_0 = 1000$. The conversion efficiency obtained in 3D simulations for $a_0 = 100$, $a_0 = 500$, and $a_0 = 1000$ is displayed together with the 2D results in Fig. 8. The absorption is somewhat lower in 3D (as the average laser intensity is lower), but is on the same order of magnitude, and so the conclusions regarding the different regimes of interaction are consistent with these results as well.

V. CONCLUSION

We have shown that it is possible to convert most of the energy from the laser (or interacting electrons in a laser-electron scattering) to γ-rays in near-future laser experiments. To achieve a strong conversion efficiency, one should either use a solid-density thin target or use intensities that can initiate a QED cascade that produces enough pairs to increase the plasma density during the interaction ($a_0 \sim 1000$). It is also possible to obtain radiation emission in controlled conditions. Using cryogenic targets, this is possible for $a_0 \sim 500$, where the number of particles is not expected to increase more than twice due to the

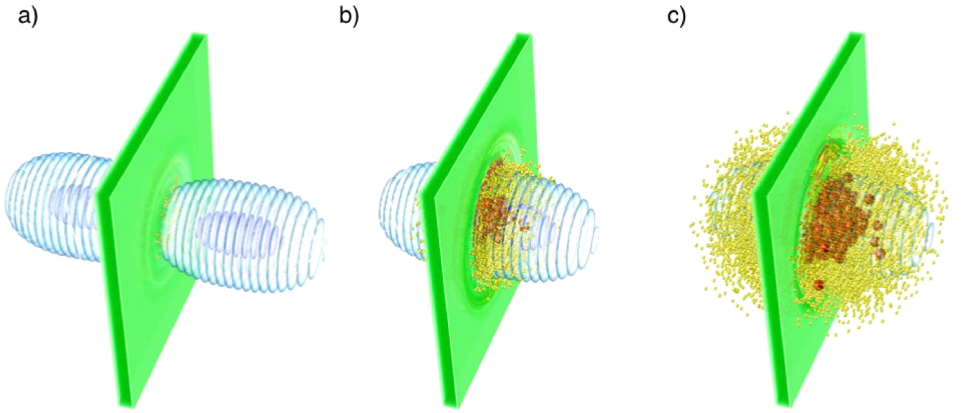

FIG. 9. 3D simulation of a two laser cascade produced using a cryogenic ice target and two lasers of $a_0 = 1000$. Half of the total laser energy is converted to γ-rays.

pair production, and the target density $n \sim 10\ n_c$ is small enough to keep the radiative absorption below 10%.

ACKNOWLEDGMENTS

This work was supported by the European Research Council (ERC-2015-AdG Grant No. 695088), Portuguese Science Foundation (FCT) Grant No. SFRH/BPD/119642/2016, and German Research Foundation (DFG) Grant No. 361969338. We acknowledge PRACE for awarding access to MareNostrum based in the Barcelona Supercomputing Center. Simulations were performed at the IST cluster (Lisbon, Portugal) and MareNostrum (Spain).

APPENDIX: SIMULATION METHODS AND PARAMETERS

All simulations are performed with the QED module of OSIRIS.[72] The QED module is a Monte Carlo module that accounts for the photon emission and Breit-Wheeler pair production and is implemented as an addition to the standard PIC loop of OSIRIS. Energetic photons are initialized as an additional particle species. The emission rates are found in Refs. 73–75. OSIRIS QED has been used previously in Refs. 16, 29, 44, 47, and 76. A similar method for incorporating BW pair production is used in several other codes.[28,31,32,34–38,77]

The simulations from Sec. III displayed in Fig. 7 are performed with parameters as in the work of Vranic *et al.*[16] The electron beam initial energy is 0.85 GeV, and initial beam divergence is $p_\perp/p_\parallel \sim 0.2$ mrad. The laser is transversely a plane wave with a temporal envelope. The total pulse duration is given by $\tau = \tau_{\text{flat}} + (\tau_{\text{rise}} + \tau_{\text{fall}})/2$, where τ_{flat} is the constant amplitude section of the wave that was varied from 0 to 160 fs. The envelope function has a smooth rise and fall, the same for all the simulations: $\tau_{\text{rise}} = \tau_{\text{fall}} = 26.6$ fs. The simulations are performed in 2D, with a box size of $500 \times 20\, c^2/\omega_0^2$ resolved with 5000×200 cells and the time step $dt = 0.04\, \omega_0^{-1}$ using 16 particles per cell (ppc).

Section IV has several types of simulations. Ideal simulations displayed in Figs. 3, 4, and 7 were performed with no current deposition and pair production: the standing wave is undisturbed by the presence of the plasma and the plasma density does not grow due to the new particle generation. The transverse boundary conditions are periodic. The simulation box size is $200 \times 10\, c^2/\omega_0^2$, resolved with 2000×100 cells and 9 ppc. The plasma slab is 1 μm thick and is composed of electrons and positrons. The initial density is $n = 0.001 n_c$. The two lasers have a 2-cycle smooth rise and fall and a 10-cycle flat section. All the measurements in ideal conditions were taken, while all particles are fully immersed in the flat-top section of the standing wave.

The 2D and 3D simulations shown in Figs. 7–9 are performed including all options of the QED PIC module. In 2D (3D), the box size was $200 \times 192\, c^2/\omega_0^2$ ($200 \times 192 \times 192\, c^3/\omega_0^3$), resolved with 2000×1920 ($2000 \times 960 \times 960$) cells and 9 ppc (27 ppc). The time step is $dt = 0.005\, \omega_0^{-1}$, and boundary conditions are open in all directions. The two laser pulses have a Gaussian transverse profile, with a spot size of $W_0 = 3\ \mu$m. The temporal envelope slope is defined by a polynomial function $f(t) = 10(t/\tau_0)^3 - 15(t/\tau_0)^4 + 6(t/\tau_0)^5$, where the pulse duration is $\tau_0 = 25$ fs. The plasma slab is initially 1 μm wide, with a density of $n = 10 n_c$, and composed of either electrons and positrons or electrons and protons.

REFERENCES

[1] K. Ta Phuoc, S. Corde, C. Thaury, V. Malka, A. Tafzi, J. P. Goddet, R. C. Shah, S. Sebban, and A. Rousse, "All-optical Compton gamma-ray source," Nat. Photonics **6**, 308–311 (2012).
[2] G. Sarri, D. J. Corvan, W. Schumaker, J. M. Cole, A. Di Piazza, H. Ahmed, C. Harvey, C. H. Keitel, K. Krushelnick, S. P. D. Mangles, Z. Najmudin, D. Symes, A. G. R. Thomas, M. Yeung, Z. Zhao, and M. Zepf, "Ultrahigh brilliance multi-MeV γ-ray beams from nonlinear relativistic Thomson scattering," Phys. Rev. Lett. **113**, 224801 (2014).
[3] S. Chen, N. D. Powers, I. Ghebregziabher, C. M. Maharjan, C. Liu, G. Golovin, S. Banerjee, J. Zhang, N. Cunningham, A. Moorti, S. Clarke, S. Pozzi, and D. P. Umstadter, "MeV-energy x rays from inverse Compton scattering with laser-wakefield accelerated electrons," Phys. Rev. Lett. **110**, 155003 (2013).
[4] N. D. Powers, I. Ghebregziabher, G. Golovin, C. Liu, S. Chen, S. Banerjee, J. Zhang, and D. P. Umstadter, "Quasi-monoenergetic and tunable x-rays from a laser-driven Compton light source," Nat. Photonics **8**, 28–31 (2014).
[5] K. Khrennikov, J. Wenz, A. Buck, J. Xu, M. Heigoldt, L. Veisz, and S. Karsch, "Tunable all-optical quasi monochromatic Thomson x-ray source in the nonlinear regime," Phys. Rev. Lett. **114**, 195003 (2015).
[6] F. Albert and A. G. R. Thomas, "Applications of laser wakefield accelerator-based light sources," Plasma Phys. Controlled Fusion **58**, 103001 (2016).
[7] W. Yan, C. Fruhling, G. Golovin, D. Haden, J. Luo, P. Zhang, B. Zhao, J. Zhang, C. Liu, M. Chen, S. Chen, S. Banerjee, and D. Umstadter, "High-order multiphoton Thomson scattering," Nat. Photonics **11**, 514–520 (2017).
[8] J. M. Cole, K. T. Behm, E. Gerstmayr, T. G. Blackburn, J. C. Wood, C. D. Baird, M. J. Duff, C. Harvey, A. Ilderton, A. S. Joglekar, K. Krushelnick, S.

Kuschel, M. Marklund, P. McKenna, C. D. Murphy, K. Poder, C. P. Ridgers, G. M. Samarin, G. Sarri, D. R. Symes, A. G. R. Thomas, J. Warwick, M. Zepf, Z. Najmudin, and S. P. D. Mangles, "Experimental evidence of radiation reaction in the collision of a high-intensity laser pulse with a laser-wakefield accelerated electron beam," Phys. Rev. X **8**, 011020 (2018).

[9]K. Poder, M. Tamburini, G. Sarri, A. Di Piazza, S. Kuschel, C. D. Baird, K. Behm, S. Bohlen, J. M. Cole, D. J. Corvan, M. Duff, E. Gerstmayr, C. H. Keitel, K. Krushelnick, S. P. D. Mangles, P. McKenna, C. D. Murphy, Z. Najmudin, C. P. Ridgers, G. M. Samarin, D. R. Symes, A. G. R. Thomas, J. Warwick, and M. Zepf, "Experimental signatures of the quantum nature of radiation reaction in the field of an ultraintense laser," Phys. Rev. X **8**, 031004 (2018).

[10]M. Vranic, J. L. Martins, J. Vieira, R. A. Fonseca, and L. O. Silva, "All-optical radiation reaction at 10^{21} W/cm^2," Phys. Rev. Lett. **113**, 134801 (2014).

[11]T. G. Blackburn, C. P. Ridgers, J. G. Kirk, and A. R. Bell, "Quantum radiation reaction in laser-electron-beam collisions," Phys. Rev. Lett. **112**, 015001 (2014).

[12]N. Neitz and A. D. Piazza, "Stochasticity effects in quantum radiation reaction," Phys. Rev. Lett. **111**, 054802 (2013).

[13]A. Di Piazza, K. Z. Hatsagortsyan, and C. H. Keitel, "Quantum radiation reaction effects in multiphoton Compton scattering," Phys. Rev. Lett. **105**, 220403 (2010).

[14]V. Dinu, C. Harvey, A. Ilderton, M. Marklund, and G. Torgrimsson, "Quantum radiation reaction: From interference to incoherence," Phys. Rev. Lett. **116**, 044801 (2016).

[15]S. R. Yoffe, Y. Kravets, A. Noble, and D. A. Jaroszynski, "Longitudinal and transverse cooling of relativistic electron beams in intense laser pulses," New J. Phys. **17**, 053025 (2015).

[16]M. Vranic, T. Grismayer, R. A. Fonseca, and L. O. Silva, "Quantum radiation reaction in head-on laser-electron beam interaction," New J. Phys. **18**, 073035 (2016).

[17]C. P. Ridgers, T. G. Blackburn, D. Del Sorbo, L. E. Bradley, C. Slade-Lowther, C. D. Baird, S. P. D. Mangles, P. McKenna, M. Marklund, C. D. Murphy *et al.*, "Signatures of quantum effects on radiation reaction in laser-electron-beam collisions," J. Plasma Phys. **83**, 715830502 (2017).

[18]F. Niel, C. Riconda, F. Amiranoff, R. Duclous, and M. Grech, "From quantum to classical modeling of radiation reaction: A focus on stochasticity effects," Phys. Rev. E **97**, 043209 (2018).

[19]A. Di Piazza, C. Muller, K. Z. Hatsagortsyan, and C. H. Keitel, "Extremely high-intensity laser interactions with fundamental quantum systems," Rev. Mod. Phys. **84**, 1177–1228 (2012).

[20]W. P. Leemans, A. J. Gonsalves, H.-S. Mao, K. Nakamura, C. Benedetti, C. B. Schroeder, C. Tóth, J. Daniels, D. E. Mittelberger, S. S. Bulanov, J.-L. Vay, C. G. R. Geddes, and E. Esarey, "Multi-GeV electron beams from capillary-discharge-guided subpetawatt laser pulses in the self-trapping regime," Phys. Rev. Lett. **113**, 245002 (2014).

[21]D. L. Burke, R. C. Field, G. Horton-Smith, J. E. Spencer, D. Walz, S. C. Berridge, W. M. Bugg, K. Shmakov, A. W. Weidemann, C. Bula, K. T. McDonald, E. J. Prebys, C. Bamber, S. J. Boege, T. Koffas, T. Kotseroglou, A. C. Melissinos, D. D. Meyerhofer, D. A. Reis, and W. Ragg, "Positron production in multiphoton light-by-light scattering," Phys. Rev. Lett. **79**, 1626–1629 (1997).

[22]M. Lobet, X. Davoine, E. d'Humières, and L. Gremillet, "Generation of high-energy electron-positron pairs in the collision of a laser-accelerated electron beam with a multipetawatt laser," Phys. Rev. Accel. Beams **20**, 043401 (2017).

[23]X.-L. Zhu, T.-P. Yu, Z.-M. Sheng, Y. Yin, I. C. E. Turcu, and A. Pukhov, "Dense GeV electron–positron pairs generated by lasers in near-critical-density plasmas," Nat. Commun. **7**, 13686 (2016).

[24]J. G. Kirk, A. R. Bell, and I. Arka, "Pair production in counter-propagating laser beams," Plasma Phys. Controlled Fusion **51**, 085008 (2009).

[25]A. Zhidkov, S. Masuda, S. S. Bulanov, J. Koga, T. Hosokai, and R. Kodama, "Radiation reaction effects in cascade scattering of intense, tightly focused laser pulses by relativistic electrons: Classical approach," Phys. Rev. Spec. Top. Accel. Beams **17**, 054001 (2014).

[26]A. R. Bell and J. G. Kirk, "Possibility of prolific pair production with high-power lasers," Phys. Rev. Lett. **101**, 200403 (2008).

[27]S. Bulanov, N. Narozhny, V. Mur, and V. Popov, "Electron-positron pair production by electromagnetic pulses," J. Exp. Theor. Phys. **102**, 9–23 (2006).

[28]E. N. Nerush, I. Y. Kostyukov, A. M. Fedotov, N. B. Narozhny, N. V. Elkina, and H. Ruhl, "Laser field absorption in self-generated electron-positron pair plasma," Phys. Rev. Lett. **106**, 035001 (2011).

[29]T. Grismayer, M. Vranic, J. L. Martins, R. A. Fonseca, and L. O. Silva, "Laser absorption via quantum electrodynamics cascades in counter propagating laser pulses," Phys. Plasmas **23**, 056706 (2016).

[30]A. A. Mironov, A. M. Fedotov, and N. B. Narozhnyi, "Generation of quantum-electrodynamic cascades in oblique collisions of ultrarelativistic electrons with an intense laser field," Quantum Electron. **46**, 305 (2016).

[31]M. Lobet, E. d'Humières, M. Grech, C. Ruyer, X. Davoine, and L. Gremillet, "Modeling of radiative and quantum electrodynamics effects in pic simulations of ultra-relativistic laser-plasma interaction," J. Phys.: Conf. Ser. **688**, 012058 (2016).

[32]M. Lobet, C. Ruyer, A. Debayle, E. d'Humières, M. Grech, M. Lemoine, and L. Gremillet, "Ultrafast synchrotron-enhanced thermalization of laser-driven colliding pair plasmas," Phys. Rev. Lett. **115**, 215003 (2015).

[33]M. Vranic, T. Grismayer, J. Martins, R. Fonseca, and L. Silva, "Particle merging algorithm for pic codes," Comput. Phys. Commun. **191**, 65– 73 (2015).

[34]N. V. Elkina, A. M. Fedotov, I. Y. Kostyukov, M. V. Legkov, N. B. Narozhny, E. N. Nerush, and H. Ruhl, "Qed cascades induced by circularly polarized laser fields," Phys. Rev. Spec. Top. Accel. Beams **14**, 054401 (2011).

[35]C. P. Ridgers, C. S. Brady, R. Duclous, J. G. Kirk, K. Bennett, T. D. Arber, A. P. L. Robinson, and A. R. Bell, "Dense electron-positron plasmas and ultraintense gamma rays from laser-irradiated solids," Phys. Rev. Lett. **108**, 165006 (2012).

[36]R. Duclous, J. G. Kirk, and A. R. Bell, "Monte Carlo calculations of pair production in high-intensity laser-plasma interactions," Plasma Phys. Controlled Fusion **53**, 015009 (2011).

[37]A. Gonoskov, S. Bastrakov, E. Efimenko, A. Ilderton, M. Marklund, I. Meyerov, A. Muraviev, A. Sergeev, I. Surmin, and E. Wallin, "Extended particle-in-cell schemes for physics in ultrastrong laser fields: Review and developments," Phys. Rev. E **92**, 023305 (2015).

[38]V. F. Bashmakov, E. N. Nerush, I. Y. Kostyukov, A. M. Fedotov, and N. B. Narozhny, "Effect of laser polarization on quantum electrodynamical cascading," Phys. Plasmas **21**, 013105 (2014).

[39]*ELI Science and Technology with Ultra-Intense Lasers WHITEBOOK*, edited by Andreas Thoss (2011).

[40]T. Heinzl and A. Ilderton, "Exploring high-intensity QED at ELI," Eur. Phys. J. D **55**, 359–364 (2009).

[41]I. C. E. Turcu, F. Negoita, D. A. Jaroszynski, P. McKenna, S. Balascuta, D. Ursescu, I. Dancus, M. O. Cernaianu, M. V. Tataru, P. Ghenuche, D. Stutman, A. Boianu, M. Risca, M. Toma, C. Petcu, G. Acbas, S. R. Yoffe, A. Noble, B. Ersfeld, E. Brunetti, R. Capdessus, C. Murhphy, C. P. Ridgers, D. Neely, S. P. D. Mangles, R. J. Gray, A. G. R. Thomas, J. G. Kirk, A. Ilderton, M. Marklund, D. F. Gordon, B. Hafizi, D. Kaganovich, J. P. Palastro, E. D'Humieres, M. Zepf, G. Sarri, H. Gies, F. Karbstein, J. Schreiber, G. G. Paulus, B. Dromey, C. Harvey, A. Di Piazza, C. H. Keitel, M. C. Kaluza, S. Gales, and N. V. Zamfir, "High field physics and QED experiments at ELI-Np," Rom. Rep. Phys. **68**, S146 (2016), see http://www.rrp.infim.ro/2016_68_S/S145.pdf.

[42]S. Weber, S. Bechet, S. Borneis, L. Brabec, M. Bučka, E. Chacon-Golcher, M. Ciappina, M. DeMarco, A. Fajstavr, K. Falk, E.-R. Garcia, J. Grosz, Y.-J. Gu, J.-C. Hernandez, M. Holec, P. Janečka, M. Jantač, M. Jirka, H. Kadlecova, D. Khikhlukha, O. Klimo, G. Korn, D. Kramer, D. Kumar, T. Lastovička, P. Lutoslawski, L. Morejon, V. Olšovcová, M. Rajdl, O. Renner, B. Rus, S. Singh, M. Šmid, M. Sokol, R. Versaci, R. Vrána, M. Vranic, J. Vyskočil, A. Wolf, and Q. Yu, "P3: An installation for high-energy density plasma physics and ultra-high intensity laser-matter interaction at ELI-beamlines," Matter Radiat. Extremes **2**, 149–176 (2017).

[43]E. G. Gelfer, A. A. Mironov, A. M. Fedotov, V. F. Bashmakov, E. N. Nerush, I. Y. Kostyukov, and N. B. Narozhny, "Optimized multibeam configuration for observation of QED cascades," Phys. Rev. A **92**, 022113 (2015).

[44]M. Vranic, T. Grismayer, R. A. Fonseca, and L. O. Silva, "Electron-positron cascades in multiple-laser optical traps," Plasma Phys. Controlled Fusion **59**, 014040 (2017).

[45]A. Gonoskov, A. Bashinov, S. Bastrakov, E. Efimenko, A. Ilderton, A. Kim, M. Marklund, I. Meyerov, A. Muraviev, and A. Sergeev, "Ultrabright GeV photon source via controlled electromagnetic cascades in laser-dipole waves," Phys. Rev. X **7**, 041003 (2017).

[46]M. Jirka, O. Klimo, S. V. Bulanov, T. Z. Esirkepov, E. Gelfer, S. S. Bulanov, S. Weber, and G. Korn, "Electron dynamics and γ and e^-e^+ production by colliding laser pulses," Phys. Rev. E **93**, 023207 (2016).
[47]T. Grismayer, M. Vranic, J. L. Martins, R. A. Fonseca, and L. O. Silva, "Seeded QED cascades in counter propagating laser pulses," Phys. Rev. E **95**, 023210 (2017).
[48]I. Y. Kostyukov and E. N. Nerush, "Production and dynamics of positrons in ultrahigh intensity laser-foil interactions," Phys. Plasmas **23**, 093119 (2016).
[49]M. Jirka, O. Klimo, M. Vranic, S. Weber, and G. Korn, "QED cascade with 10 pw-class lasers," Sci. Rep. **7**, 15302 (2017).
[50]B. Martinez, E. d'Humières, and L. Gremillet, "Synchrotron emission from nanowire array targets irradiated by ultraintense laser pulses," Plasma Phys. Controlled Fusion **60**, 074009 (2018).
[51]S. Meuren, C. H. Keitel, and A. Di Piazza, "Semiclassical picture for electron-positron photoproduction in strong laser fields," Phys. Rev. D **93**, 085028 (2016).
[52]APOLLON, http://www.apollon-laser.fr/.
[53]CoReLS, https://corels.ibs.re.kr/html/corels_en/.
[54]FACET-II, https://portal.slac.stanford.edu/sites/ard_public/facet/Pages/FACET-II.aspx.
[55]R. Assmann, T. Behnke, B. Heinemann, J. List, J. Negodin, A. Ringwald, M. Altarelli, A. Hartin, and M. Wing, https://indico.cern.ch/event/644287/contributions/2763845/attachments/1563012/2461684/LUXE_Wing.pdf (2017).
[56]A. Hartin, A. Ringwald, and N. Tapia, "Measuring the boiling point of the vacuum of quantum electrodynamics," Phys. Rev. D **99**, 036008 (2019).
[57]S. Meuren, "Nonlinear quantum electrodynamic and electroweak processes in strong laser fields," Ph.D. thesis (Combined Faculties of the Natural Sciences and Mathematics of the Ruperto-Carola-University of Heidelberg, Germany, 2015).
[58]L. S. Brown and T. W. B. Kibble, "Interaction of intense laser beams with electrons," Phys. Rev. **133**, A705–A719 (1964).
[59]T. W. B. Kibble, "Frequency shift in high-intensity Compton scattering," Phys. Rev. **138**, B740–B753 (1965).
[60]V. Ritus, "Quantum effects of the interaction of elementary particles with an intense electromagnetic field," J. Sov. Laser Res. **6**, 497–617 (1985).
[61]V. B. Berestetskii, L. D. Landau, E. M. Lifshitz, and, and L. Pitaevskii, *Quantum Electrodynamics* (Butterworth-Heinemann, 1982), Vol. 4.
[62]V. Yakimenko, S. Meuren, F. Del Gaudio, C. Baumann, A. Fedotov, F. Fiuza, T. Grismayer, M. Hogan, A. Pukhov, L. Silva *et al.*, "On the prospect of studying nonperturbative QED with beam-beam collisions," preprint arXiv:1807.09271 (2018).
[63]V. Baier and V. Katkov, "Processes involved in the motion of high energy particles in a magnetic field," Sov. Phys. JETP **26**, 854 (1968) see, http://www.jetp.ac.ru/cgi-bin/dn/e_026_04_0854.pdf.
[64]F. Mackenroth and A. Di Piazza, "Nonlinear Compton scattering in ultrashort laser pulses," Phys. Rev. A **83**, 032106 (2011).
[65]A. M. Fedotov, N. B. Narozhny, G. Mourou, and G. Korn, "Limitations on the attainable intensity of high power lasers," Phys. Rev. Lett. **105**, 080402 (2010).
[66]T. Z. Esirkepov, S. S. Bulanov, J. K. Koga, M. Kando, K. Kondo, N. N. Rosanov, G. Korn, and S. V. Bulanov, "Attractors and chaos of electron dynamics in electromagnetic standing waves," Phys. Lett. A **379**, 2044– 2054 (2015).
[67]J. T. Mendonça, "Threshold for electron heating by two electromagnetic waves," Phys. Rev. A **28**, 3592–3598 (1983).
[68]I. Y. Kostyukov, I. Artemenko, and E. Nerush, "Growth rate of QED cascades in a rotating electric field," Probl. At. Sci. Technol. **116**(4), 259–263 (2018).
[69]M. Tamburini, A. Di Piazza, and C. H. Keitel, "Laser-pulse-shape control of seeded QED cascades," Sci. Rep. **7**, 5694 (2017).
[70]L. Obst, S. Göde, M. Rehwald, F.-E. Brack, J. Branco, S. Bock, M. Bussmann, T. E. Cowan, C. B. Curry, F. Fiuza *et al.*, "Efficient laser-driven proton acceleration from cylindrical and planar cryogenic hydrogen jets," Sci. Rep. **7**, 10248 (2017).
[71]A. Tebartz, S. Bedacht, M. Hesse, S. Astbury, R. Clarke, A. Ortner, G. Schaumann, F. Wagner, D. Neely, and M. Roth, "Creation and characterization of free-standing cryogenic targets for laser-driven ion acceleration," Rev. Sci. Instrum. **88**, 093512 (2017).
[72]R. A. Fonseca, L. O. Silva, F. S. Tsung, V. K. Decyk, W. Lu, C. Ren, W. B. Mori, S. Deng, S. Lee, T. Katsouleas, and J. C. Adam, *Lecture Notes on Computer Science* (Springer, Berlin/Heidelberg, 2002), Vol. 2331, pp. 342–351.
[73]A. I. Nikishov and V. I. Ritus, "Pair production by a photon and photon emission by an electron in the field of ultra intense electromagnetic wave and in a constant field," Sov. Phys. JETP **25**, 1135 (1967), see http://www.jetp.ac.ru/cgi-bin/dn/e_025_06_1135.pdf.
[74]V. Baier and V. Katkov, "Quantum effects in magnetic Bremsstrahlung," Phys. Lett. A **25**, 492– 493 (1967).
[75]N. P. Klepikov, "Emission of photons or electron-positron pairs in magnetic fields," Zhur. Eksptl. Teoret. Fiz. **26**, 27–44 (1954).
[76]M. Vranic, O. Klimo, G. Korn, and S. Weber, "Multi-GeV electron-positron beam generation from laser-electron scattering," Sci. Rep. **8**, 4702 (2018).
[77]A. Gonoskov, A. Bashinov, I. Gonoskov, C. Harvey, A. Ilderton, A. Kim, M. Marklund, G. Mourou, and A. Sergeev, "Anomalous radiative trapping in laser fields of extreme intensity," Phys. Rev. Lett. **113**, 014801 (2014).